BRILLOUIN SCATTERING SPECTROSCOPY AND MICROSCOPY:

TECHNIQUES AND APPLICATIONS

An Undergraduate Research Scholars Thesis

by

ZACHARY ANDREW STEELMAN

Submitted to Honors and Undergraduate Research
Texas A&M University
in partial fulfillment of the requirements for the designation as an

UNDERGRADUATE RESEARCH SCHOLAR

Approved by
Research Advisor: Dr. Vladislav Yakovlev

May 2014

Major: Biomedical Engineering

TABLE OF CONTENTS

ABSTRACT

Brillouin Scattering Spectroscopy and Microscopy: Techniques and Applications. (May 2014)

Zachary Andrew Steelman
Department of Biomedical Engineering
Texas A&M University

Research Advisor: Dr. Vladislav Yakovlev
Department of Biomedical Engineering

Brillouin Spectroscopy is a widely used optical technique for material characterization and analysis. Recent studies suggest that Brillouin spectroscopy can be extended into an imaging modality, which would present with a wide range of applications in the study of biomechanics, stem cell differentiation, and cancer diagnostics. Extending this technology to microscopy would represent a significant advancement in optical imaging technology, in addition to a substantial capacity for commercialization. We show the potential use of Brillouin spectroscopy as a diagnostic tool for bacterial meningitis, improve the Brillouin spectrum using molecular absorption cells to filter elastically scattered photons, and develop existing Brillouin spectroscopy technology into imaging with Brillouin microscopy to create two-dimensional images of soft tissue on the micro-scale by the tissue's bulk modulus or compressibility. In this way, we offer a method by which microscopic changes in the solid mechanical properties of tissue can be monitored, leading to a better understanding of the ways in way forces direct biological tissue to differentiate and change.

DEDICATION

I dedicate this research to my parents. Without their continued support this opportunity would

not have been possible.

ACKNOWLEDGEMENTS

NOMENCLATURE

CSF Cerebrospinal Fluid

2D Two Dimensional

3D Three Dimensional

VIPA Virtually Imaged Phased Array

CHAPTER I

INTRODUCTION

Biomechanics has proven to be an influential field of study with significant applications in regenerative medicine, especially pertaining to stem cell differentiation (Engler, Sen et al. 2006). In fact, improved knowledge of the mechanical properties and interactions of living tissue has led to a better understanding of critical disease progression, including prominent research in coronary artery and cardiovascular disease. Biomechanics of the body's soft and hard tissues plays a critical role in day-to-day tissue functionality as well; overall, research continues to uncover the importance of biomechanical interactions. However, the study of these interactions brings along a host of challenges, due primarily to the understudied nature of the field. New techniques are needed which can accurately and comprehensively evaluate mechanical tissue interactions on both a small and large scale. Brillouin spectroscopy offers one such solution. Brillouin spectroscopy, while traditionally used to study nonliving material properties, has shown the remarkable ability to determine mechanical properties of tissues without deforming them, making it a powerful tool for the study of mechanical interactions in tissue. (Bailey, Twa et al. 2010) However, the development of Brillouin spectroscopy, particularly in the use of micro-scale imaging, still requires significant development in order to make the leap from laboratory research tool to clinical diagnostic modality. This is a significant limitation to current technology and scientific understanding, as Brillouin scattering offers an immeasurably high ceiling in terms of the quality and quantity of biomechanical information that it can provide to researchers and health care professionals. We propose to not only find clinically relevant

applications for Brillouin spectroscopy, but also to develop Brillouin microscopy, and apply it to the biomechanics of soft tissues. While there exist a plethora of applications including (but not limited to) the study of micro-imperfections in bone graft structures, the mechanical factors that influence stem cell differentiation, and potential applications in highly accurate cancer diagnostics, in this thesis, we primarily present two developments; initially, we show one of the first applications of Brillouin spectroscopy from a pure diagnostics standpoint by showcasing its ability to detect increased protein concentration in cerebrospinal fluid (CSF) indicative of bacterial meningitis, and second, we show our own development of Brillouin microscopy and its applications to micro-scale imaging and sensing. Along the way, we will showcase small improvements (in particular, notch filtering of elastic scattering using a molecular absorption cell) that we have made to current Brillouin spectroscopy setups, and the effect that these improvements have had upon our data acquisition and measurement during the aforementioned applications.

Brillouin spectroscopy itself is not an entirely new concept. Studies have been performed for the past few decades using Brillouin spectroscopy as a tool to sense the modulus of a material without forming a stress-strain plot, and most importantly, without applying a force. Instead, Brillouin scattering (which is the information collected in Brillouin spectroscopy) can be thought of as a Doppler-shifted interaction between incoming radiation (photons) with sound waves (acoustic phonons) in the material. As a sound wave (or, in a better sense, a compression wave) passes through a material, the index of refraction at the crest of the wave changes. In addition, the material becomes more highly reflective at the point of compression along the wave. Due to these effects, light is scattered at a slightly higher incidence than it otherwise would at the crest

of the wave. In addition, because the sound wave is traveling at a certain speed within the

material (which is highly dependent on the material's mechanical properties), there is a slight

Doppler shift between the incident light and the Brillouin shifted portion of the scattered light,

typically on the order of 5-10 GHz (this is on the scale of a difference of picometers, which is

very small and can be difficult to detect. The Brillouin frequency shift is directly proportional to

both the index of refraction and the square root of the bulk modulus of the material, and

inversely proportional to the square root of the material's density. Since refractive index, bulk

modulus, and density can all be temperature dependent, Brillouin scattering has also been used as

a tool for remote temperature sensing. The complete expression for the Brillouin frequency shift

of light is given by

$$v = \frac{2n}{\lambda} \sqrt{\frac{B}{\rho}} \cos\left(\frac{\theta}{2}\right)$$

Where v is the frequency shift of incoming versus scattered light (in Hertz), n is the refractive

index of the material, λ is the wavelength of the incident light, B is the bulk or elastic modulus of

the material for fluids and solids, respectively, ρ is the density of the medium, and θ is the angle

of scattering. For backscattered light, $\theta=\pi$. It is also very important to note that the quantity $\sqrt{\frac{B}{\rho}}$

in the equation represents the speed of sound in a given medium, showing the dependence of a

material's internal sound velocity on its corresponding Brillouin frequency shift. The exact

formulation of the Brillouin frequency shift allows for an array of information to be obtained

from a given sample.

Because of this unique relation, Brillouin scattering has been used for a number of purposes. As stated above, since n is usually a function of temperature (as is the bulk modulus) Brillouin scattering has been used as a tool to remotely sense for the temperature of substances, for example, ocean water. Sound velocity measurement within certain materials is also a unique and potentially powerful application for Brillouin spectroscopy, as internal sound velocity garners a large amount of potential information about the sample in question and is used in a variety of scenarios. More commonly, however, Brillouin spectroscopy is used as a method to determine the bulk modulus of materials. It is highly favored in this regard for its ability to determine bulk modulus without any mechanical deformation, a feat which is unmatched by nearly any other method.

In general, the difficulty presented by Brillouin spectroscopy is that of separating the scattered portion of the light (which exhibits a very slight change in wavelength) from the elastically scattered portion (which is much stronger and does not change wavelength). In the past, Fabry-Perot interferometers have been used primarily as a method of separating the wavelengths, however, recent advancements in methodology and instrumentation offer a much better solution. In particular, we have opted to use the multi-stage VIPA (virtually imaged phased array) approach as reported in the literature. This method has been very successful in separating wavelengths radially, and is currently the best approach known. This is primarily due to actions of the VIPA etalons, which create interference patterns of a collimated laser beam and output spatial images whose appearances are highly sensitive to wavelength shifts. We propose to apply this technique to a number of soft tissue and biofluid applications in order to obtain both

point-source information, as well as diagnostic image creation and analysis in order to further

study the biomechanics of tissues at the macroscopic and cellular level.

CHAPTER II

MATERIALS AND METHODS

Most results were obtained using a 532 nm (green) laser, but 780 nm may be better

For this particular experiment, we first employed setups for spontaneous Brillouin spectroscopy using both 780nm (near infrared) and 532 nm (green) continuous single-mode lasers. Preliminary studies and results were performed primarily using the 532nm laser, and indeed, most results were obtained from this setup. However, it must be noted that for biological and biomedical applications, 780nm beams are vastly preferred due to their increased penetration depth and low interactivity with biological tissues. Further development of the results obtained in this thesis using a near-infrared (approximately 780 nm) source are needed, and are currently in development in ours and other research labs. We built the setups exactly as previously reported, using a 2-stage VIPA spectrometer to separate the elastic and inelastically scattered light. Further descriptions of the setup, as well as helpful illustrations, are in the following section, as well as Figures 1 and 2.
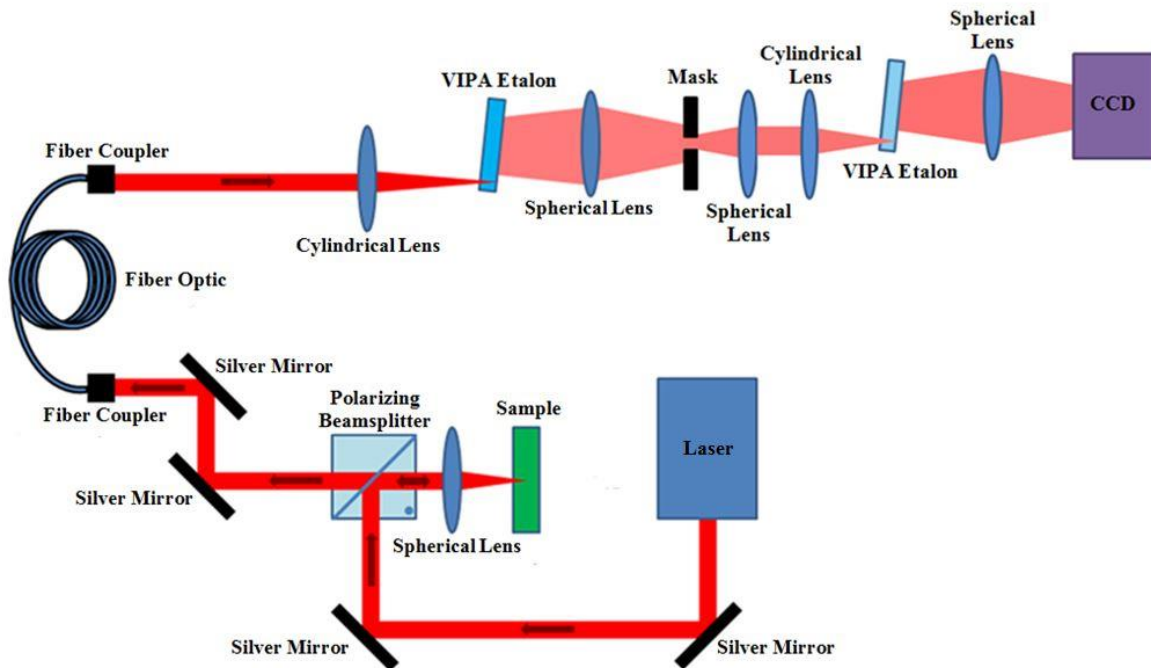
Figure 1: A basic illustration of the various spectrometer components employed, including lenses, mirrors, fiber optic cables, etc.

Brillouin spectrometer components and design

A single-mode, continuous wave laser (Lasermate Group, Inc.; model: GMSL-532-100FHA) with a measured center wavelength of 531.9587 nm ±0.3 pm was used as the incident source for Brillouin spectroscopy. The two-stage VIPA spectrometer, as was reported by Scarcelli and Yun, was used to create the Brillouin spectrum. The nominal linewidth of the 780 nm laser source was approximately 640 kHz, with a maximum output power of ~100mW. An optical isolator (Electro-Optics Technology, Inc., Model: BB-8-05-I-090) was also placed in the beam path to avoid undesirable responses within the laser cavity from unwanted reflections and scattering. This functions essentially as a one-way filter for the beam, allowing the light to pass

in the forward direction, but not allowing anything to pass back through into the source laser cavity. This is incredibly important, as even a small amount of coherent light entering a laser cavity will vastly alter the functionality and output wavelength of the source beam. The beam was then passed into a 50-50 non-polarizing beamsplitter (in a setup common to many forms of spectroscopy), an effect of which is necessarily a loss of power, but can be very useful in spectroscopic designs. After the light makes its first pass through the beamsplitter, it is focused by a microscope objective lens (Nikon, Inc., CFI Plan Fluor 20x, N.A. = 0.5) onto whatever sample the Brillouin frequency shift needs to be measured in. Samples were either placed in quartz cuvettes (Starna Cells Inc.), in the case of fluid samples, or in the case of solid samples, were placed in a microscope slide. While most light was allowed to pass completely through the sample (especially in the case of fluids) backscattered light with exactly a 180 degree scattering angle was collected back through the same objective lens, and directed into a single-mode fiber (Fibercore Inc., model: SM600, 1 meter), which passed the signal to the 2-stage VIPA spectrometer, mirroring the technique designed by Scarcelli and Yun (Scarcelli, Scarcelli et al. 2011). The single mode fiber was instrumental in collecting only perfectly backscattered photons, which allowed for a narrow output linewidth and easy spectral characterization. In fact, attempts to create a Brillouin spectrometer without employing a fiber-based setup proved to be difficult, time-consuming, and often ineffective (this is somewhat obvious from the equation from Brillouin scattering). From the fiber, the light (carrying the small Brillouin signal and a vastly greater amount of elastically scattered light), was allowed to enter into the VIPA spectrometer (VIPA etalons and associated optics). Specifically, the VIPAs (Light Machinery Inc., model: OP-5642) were chosen to possess a free spectral range of 33.3 GHz, and were fabricated explicitly for use with a laser beam of wavelength 532 nm such that one surface would

reflect 99.5% of the light at 532 nm, and the other would reflect 95%. Within the etalon, an

interference pattern is created and displayed by the 95% reflective side, which is then output to

the next VIPA etalon, the output of which represents a 2-dimensional interference pattern. To

minimize optical diffraction, 2 inch lenses were used throughout the spectrometer to ultimately

create a cleaner signal, and a 1 meter focal length lens placed after the second VIPA etalon

allowed for the Brillouin scattered light to be sufficiently separated from the elastically scattered

photons. The resulting spectrum was acquired on a CCD camera (Moravian Instruments, model:

G2-8300, pixel size 5.4 microns x 5.4 microns). A typical data acquisition time was 20 seconds

for point sampling; for imaging, each pixel consisted of 100 ms of signal acquisition. The

complete spectrometer is again shown in Figure 3, this time showcasing the placement of the

VIPA etalons (at a 90 degree angle to each other, and also at a slight tilt along the beam axis).
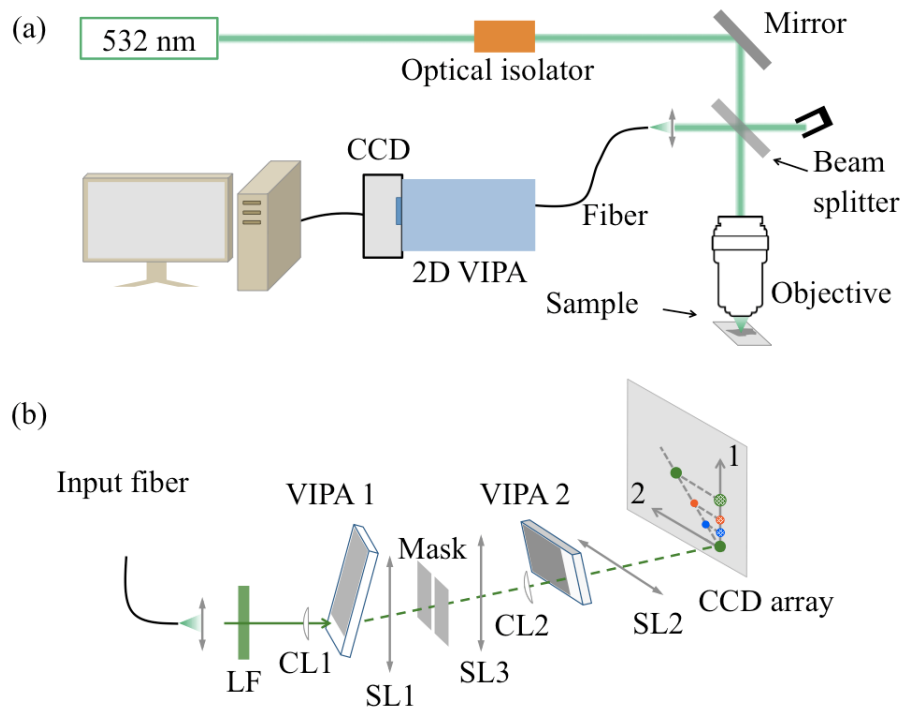
Figure 3: (a) Basic schematic diagram of a Brillouin spectrometer. (b) A more detailed schematic of a two-stage VIPA spectrometer, shown here to illustrate the placement and orientation of the VIPA etalons (LC: line filter at 532 nm, CL: cylindrical lens, SL: spherical lens).

Brillouin spectroscopy as a nondestructive screening method for bacterial meningitis

The first experiment performed was an attempt to find a direct clinical application for Brillouin spectroscopy. After some deliberation, we settled on one idea: the diagnosis of bacterial meningitis. To give some background, bacterial meningitis is a particularly challenging diagnosis for physicians from all parts of the world due to the non-specificity of symptoms, particularly in children (El Bashir, Laundy et al. 2003). It is a deadly and fast-acting disease; even with early diagnosis and adequate treatment, a 10% mortality rate still exists, often within

24-48 hours of the onset of symptoms (Swartz 2004, Mongelluzzo, Mohamad et al. 2008). If no treatment is available, as is the case in many areas, particularly within the developing world (where meningitis is an order of magnitude or more widespread), the mortality rate increases to as high as 80% (Swartz 2004). Furthermore, bacterial meningitis causes significant complications for 50% of survivors (Pfister, Feiden et al. 1993), which often leads to a decrease in life expectancy and nearly always exacerbates quality of life. A lumbar puncture (spinal tap) is generally implemented immediately upon suspicion of meningitis to obtain a sample of spinal fluid (Enwere and Obaro 2001). It is the analysis of this spinal fluid sample that is most useful in making a rapid and accurate diagnosis. Indeed, most current diagnostic tests for meningitis necessitate spinal fluid analysis, comparing the finding to external symptoms in order to make the best possible diagnosis. Rapid diagnosis and immediate treatment with antibiotics greatly reduces the mortality rate of bacterial meningitis (Tunkel and Scheld 2002), however most existing diagnostic tests of the spinal fluid are either too slow (such as bacterial cultures, which require at least 24 hours (Stuertz, Merx et al. 1998), an unacceptable timescale considering the progression of the disease) or destructive to a portion of the CSF sample obtained from *in vivo* (generally, through mixing with laboratory indicators or heavy dilution (Pennock, Passant et al. 1968, Karlsson and Alling 1980)). Because most of the traditional methods of total protein quantification require destruction of the CSF fluid, volume of sample is restricted from being used for other available tests. In addition, laboratory agents, as well as pre-testing modifications to the spinal fluid of a patient, require time and often considerable monetary cost, depending on the reagent. A method that avoids these time and cost investments would be vastly preferably, especially in an economy of overstretched hospitals and care centers.

We take particular advantage of the fact that in virtually all cases of bacterial meningitis, total protein concentrations in the CSF are elevated (Brouwer, Thwaites et al.). Therefore, detecting an increase in the total protein content of spinal fluid, along with identification of common symptoms, would be indicative of bacterial meningitis, allowing physicians to begin an immediate treatment regimen of antibiotics. Many common methods of detecting total protein, such as biuret methods and dye-binding techniques are sensitive enough to accurately detect the low levels of protein present in CSF, but require destruction of some of the CSF sample, several laboratory reagents and materials, and valuable preparation time (Karlsson and Alling 1980). Other common methods, such as UV-visible spectroscopy and other absorbance methods often require destruction of the sample by dilution, and in many cases are not appropriate due to significant error introduced by variability between different proteins (Metsämuuronen, Mänttäri et al. 2011) as well as the presence of various other molecules commonly found in biological fluids. In addition, a range of proteins exist which are elevated in the CSF, making molecule-specific tests less accurate and suggesting more of a bulk technique. Recent advances in the use of Raman microspectroscopy suggest its use for CSF tubercular meningitis diagnostics, however, early results in one particular study indicate a specificity of the new method of only 82%, with sensitivity also being an issue of concern for clinical translation (Sathyavathi, Dingari et al. 2013).

Brillouin spectroscopy offers a possible method of quantifying total protein concentration without alteration of the fluid obtained from the body. As the total protein concentration of a solution changes, so does the adiabatic elasticity of the fluid (Wang, Lee et al. 2001), expressed as bulk modulus or compressibility.

In order to determine the ability of Brillouin spectroscopy to accurately distinguish cerebrospinal fluid exhibiting increased total protein, model fluids were prepared, using similar ratios of protein, glucose, and salts to those found *in vivo* in healthy and diseased states. Samples consisted of porcine serum albumin (Sigma-Aldrich, purity $\geq$ 98%) in phosphate-buffered saline (Sigma-Aldrich, 0.01M, pH 7.4), as well as α-D-Glucose (Sigma-Aldrich, purity $\geq$96%) in concentrations made to imitate *in vivo* CSF total protein and glucose concentrations of healthy and diseased patients (Actual composition: "healthy" model: 0.27 mg/mL albumin, 0.7 mg/mL glucose; "diseased" model: 2.5 mg/mL albumin, 0.3 mg/mL glucose). Serum albumin was substituted for all proteins because of its globular structure (Monkos 2005) and prominence in diseased spinal fluid compositions. A third sample type consisting of only PBS acted as a control, and was used to calibrate the laser drift over the course of testing. Since Brillouin frequency shifts have a significant dependence on the temperature of the sample being analyzed (Haidong, Huijuan et al. 2013), all three solutions were placed in the room housing the spectrometer for several hours prior to data collection to equilibrate the samples with the room's temperature, and were then placed in quartz cuvettes, which had also been housed in the room. In order to define the sensitivity of the screening technique to larger protein concentrations (and to see the amount of improvement needed to facilitate better results), a small amount of both protein containing samples were transferred to dialysis cassettes (Slide-A-Lyzer, 2K MWCO, 3mL), which were immersed in a high molecular weight poly(ethylene glycol), MW = 3350, and allowed to dialyze on a shaker table for 100 minutes. This allowed the water and glucose in the solution to diffuse across the membrane to the highly hygroscopic poly(ethylene glycol), while the protein remained within and the solution became concentrated (due to the relatively large

nature of protein molecules compared to glucose and water molecules). Measurement of the remaining fluid volume obtained from dialysis indicated that approximately 50% of the water in the solution crossed through the membrane in all cases, leaving behind a solution of roughly double the concentration of proteins (glucose has a molecular weight of less than 200 Da, and was thus free to cross the membrane). These concentrated fluid samples were allowed to equilibrate thermally as well, and were then examined using the spectrometer. To correct for any thermal drift of the laser output wavelength (due to self-heating), three groups of ten control samples of PBS were taken at random intervals between body-similar samples, and a linear correction was made to all data points based on the best fit line of the PBS fluid samples based upon the exact time of data acquisition. For each sample tested, ten consecutive measurements were taken (including 30 total PBS control measurements). All measurements, while random, were performed consecutively so that the laser drift could be monitored on the smallest possible time scale.

Data processing and calibration for point sampling

A section of a typical spectral image, showcasing a single iteration of the full pattern of Brillouin and elastic peaks, is shown in the Figure 4, where the Brillouin peaks (Stokes and anti-Stokes) are clearly visible. The raw output images were processed using a MATLAB code which calculated the linear distance in pixels between the weighted centers (by intensity) of two corresponding Stokes and Anti-Stokes Brillouin peaks after performing background subtraction to eliminate noise and correcting for a detected laser drift. First, the algorithm computes the average signal intensity of a background region of the output image, and then normalizes each image's overall intensity to its own background to ensure accurate processing between data sets.

The algorithm then scans the image around the Brillouin peaks with a small window (approximately 60 microns by 60 microns, or 11x11 pixels), and, upon finding the area showing the strongest signal within a window, expands symmetrically into a circular region and calculates the center of that region, weighted for signal intensity. In this way, any randomly accumulated background noise (which has been observed to be as high as 75% of the Brillouin peak intensity) does not affect the center of the Brillouin peak as it would if we simply predefined a window in which to search for Brillouin spots. It is also important to note that the elastically scattered light (corresponding to the center of a given output image) is orders of magnitude stronger in intensity than the Brillouin peaks. Methods will be taken later to remove this unnecessary information from the CCD camera images to ensure accurate data processing. The linear distance between two corresponding Brillouin spots, as calculated by the algorithm, was then normalized to the drift across peak distances found in PBS control samples. The drift was found to be nearly linear in time, and was corrected using a best fit line based upon the exact time of exposure. The Brillouin peak was only slightly more intense than the background (as previously noted), while the central peak was orders of magnitude more intense, so special efforts were undertaken to eliminate noise for the camera, which was placed in an opaque black box, along with the VIPA optics and related lenses, mirrors, masks, etc.
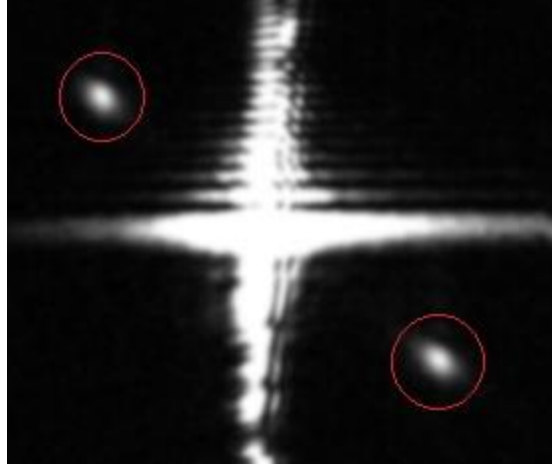
Figure 4: Typical raw CCD camera data of a 2-stage VIPA Brillouin spectrometer: inelastically scattered Brillouin peaks (circled) and elastically scattered incident radiation (center).

A significant number of studies have been performed regarding the speed of sound in water, as well as the refractive index of water, in relation to its temperature and salt content (Leyendekkers 1977, Bilaniuk and Wong 1993, Richerzhagen 1996, Carman 2012). We believed that this offered a valuable comparison tool in order to convert pixel values on a CCD to an accurate Brillouin frequency shift, the average peak-to-peak distance of PBS buffer calculated above was normalized to the expected Brillouin shift of water, using identical values for salinity and room temperature. As all other components make up less than 10% of the total dissolved solids, the NaCl concentration of the PBS solution was used for salinity in the calculation. An empirically derived formula for the speed of sound in water (Hirschberg, Byrne et al. 1984) (V) based on its temperature (T) in Celsius, and salt content (S) in parts per thousands (ppt) is given by Equation 2:

$$V = 1449 + 4.6T - 0.055T^2 + 0.003T^3 + (S - 35)(1.39 - 0.012T) \qquad (2)$$

Utilizing Equations (1) and (2), and a literature-obtained refractive index of 1.334 (Leyendekkers 1977), the mean peak-to-peak pixel distance of PBS buffer control samples was normalized to a calculated value of 7.6007 GHz. In order to maintain a consistent comparison, the arc length between adjacent elastically scattered peaks (traced along an interference line using a 3-point spline interpolation algorithm) was normalized to the free spectral range of the VIPA etalons (a value of 33.3 GHz) to determine a pixel distance/GHz conversion ratio for each image. Finally, deviations from the average PBS peak-to-peak pixel distance were converted to GHz (frequency) shift values using the calculated conversion ratios, and a Student's *t*-test was performed between each sample's data set to determine a confidence level for the screening method. Results were termed significant if the *p*-value obtained from the *t*-test was less than $\alpha=0.05$.

Notch filtering of the output using molecular absorption cells

As noted above, the elastically scattered radiation intensity is typically orders of magnitude stronger than the Brillouin peaks. Removal of the elastic radiation via notch filtering is one potential method of simplifying the analysis of Brillouin spectra, as this would drastically clean up the spectrum and allow for easier and shorter algorithms to analyze the sample. One method of notch filtering would be to use molecular absorption cells. Molecular absorption cells are essentially vacuum tubes of glass filled with a small amount of a single element or molecule, which is then heated. When the compounds within (in our case, iodine vapor) are heated, they absorb light in very narrow wavelength bands. These bands can be tuned, based upon temperature, to the wavelength of interest. We proposed to demonstrate the use of molecular absorption cells in Brillouin spectroscopy in order to remove the central elastic peaks, leaving

only the Brillouin peaks behind. In order to do this, we used a setup almost identical to what was

previously reported, except we placed a molecular absorption cell in the beam path, as depicted
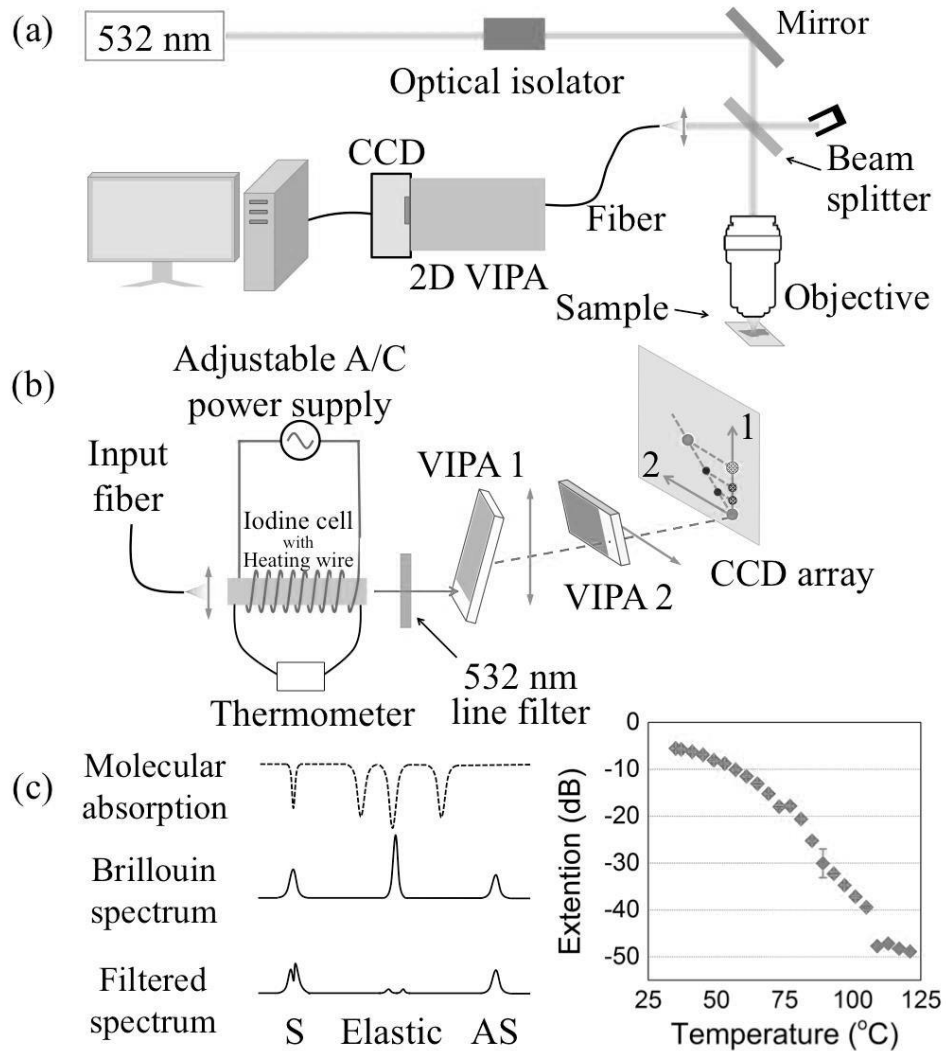
in Figure 5 below.

Figure 5: (a) Setup to include iodine molecular absorption cell. (b) Theoretical Effect of the cell

on the Brillouin Spectrum, and (c) Effect of the cell on image extinction.

In theory, the molecular absorption cell should be capable of filtering out the elastic peak,

leaving only the Brillouin peaks for analysis.

Development of Brillouin images

Lastly, we attempted to create Brillouin images; that is, modulus maps of tissue, by scanning across a solid, inhomogeneous sample. In order to do this, we simply added a translation stage to the sample holder in order to scan point-by-point within the sample and create an image. High N.A. value lenses were utilized in order to obtain a resolution of approximately 2 microns. For samples, we used chicken and pig skin, sometimes treated with acetone, in order to try and achieve an accurate modulus mapping. The same principles as before applied here, we simply scanned the sample using a high-resolution translation stage (controlled by a LabVIEW code) in order to make a "map" of the Brillouin spectrum at each point.

CHAPTER III

RESULTS

Brillouin Spectroscopy is capable of distinguishing healthy and diseased spinal fluid

Upon measurement of the fluid samples modelling healthy and diseased states, excellent distinction between different fluid models was achieved. At protein and glucose concentrations mimicking human CSF in healthy and diseased patients, the average Brillouin shift of the "diseased" fluid (7.655 GHz) showed a clear increase from that of the "healthy" fluid (7.616 GHz). In particular, a two-tailed, Student's *t*-test proved with a very high degree of confidence (P=0.014) that the two samples were distinguishable based solely upon their Brillouin shifts. Predictably, the spectra from the fluid samples which had been concentrated by dialysis showed a much more significant distinction between the "healthy" and "diseased" samples (P=5.71×10^{-5}), with mean Brillouin shifts of 7.639 and 7.719 GHz, respectively. It is also obvious that the Brillouin shift increased monotonically with protein concentration, confirming our theory and assuring validity in the test. While the distinction between "healthy" CSF and PBS was not significant (P=0.215), the diseased fluid model was clearly distinguishable from the PBS control samples, with a very high degree of confidence (P=1.35×10^{-4}). As expected, increased concentration of proteins in general increased the Brillouin frequency shift of the fluid sample, with seemingly no regard to the amount of glucose present. The results of this experiment, along with the very high degree of confidence associated with this method, make it a potentially powerful diagnostic test for CSF total protein indicative of meningococcal inflammatory diseases. All data from these tests, including *p*-values calculated using a two-tailed, equal variance *t*-test, are summarized in Figure 6.
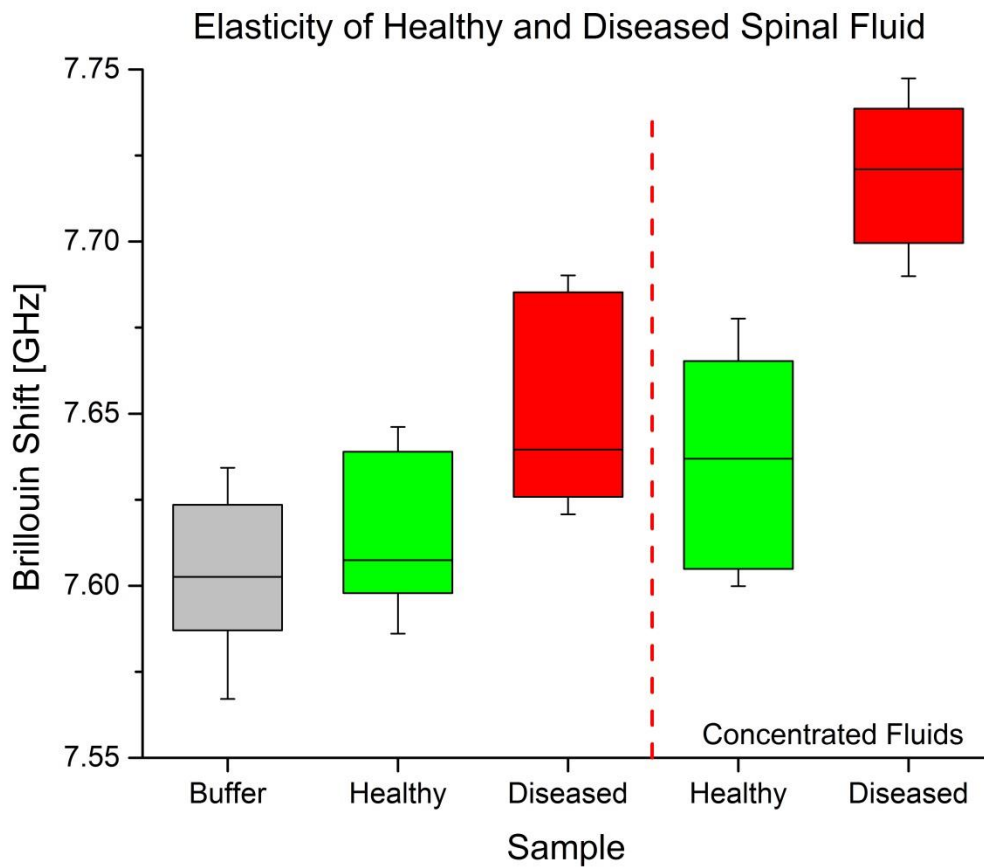
Figure 6: A very significant (P=0.014) increase in the Brillouin frequency shift of human spinal fluid is observed when protein and glucose concentrations mimic those present in fluid infected with bacterial meningitis vs. normal fluid. When the fluids are concentrated, the distinction becomes much greater. Box edges represent the middle two quartiles, and whiskers denote standard deviation.

Molecular absorption cells can filter out elastically scattered photons from the spectrum

Upon placing the molecular absorption cell into the setup, and heating to a proper temperature, we saw marked decrease in intensity of the elastic peak, sometimes removing it entirely. In fact, even with the two-dimensional configuration, the entire elastic peaks were in some cases eliminated. An illustration of the effects of the absorption cell is shown below in Figure 7.
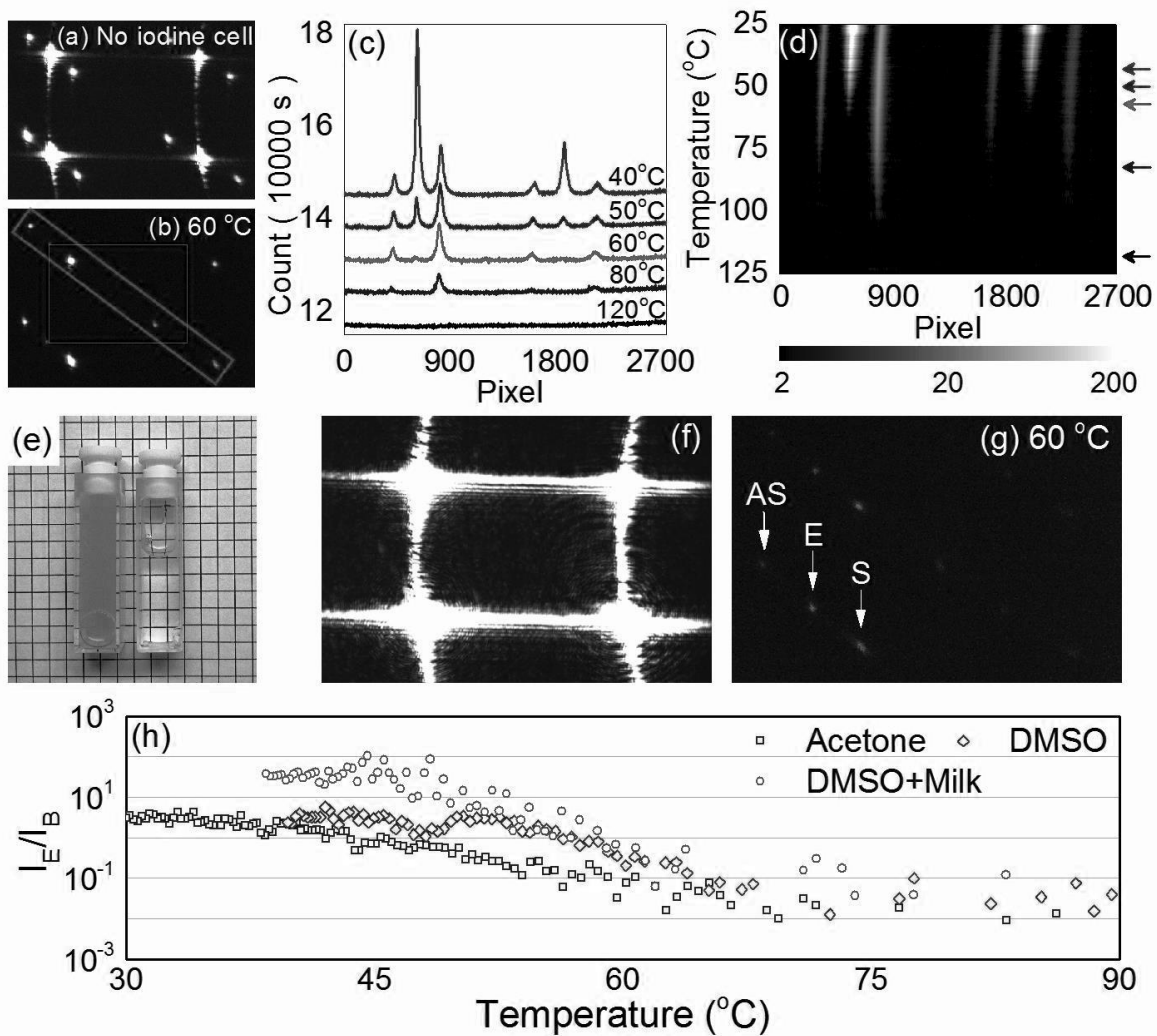

Figure 7: (a)-(d) Illustration of vast improvements to the spectrum introduction of the iodine cell has made. (f,g) Illustration of the ability to view turbid samples after cell introduction, as depicted in (e). (h) Increase in Brillouin signal with cell temperature.

It is extremely apparent that the introduction of a molecular absorption cell has vastly improved the Brillouin spectrum, and the introduction of such a cell should be included in all Brillouin systems.

The creation of Brillouin images is possible via scanning laser methods

Upon attempting to create Brillouin images, we found that we were markedly successful in our endeavor. Adding nothing more to the system but a simple translation stage, we have been able to create two-dimensional Brillouin images of the moduli of soft tissues with a resolution of approximately 2 microns. While we saw significant laser drift within the samples, small corrections, perhaps via a side system which senses a control sample, would allow for the correction of this drift. This represents the newest direction for our project, which we hope will create much better images. However, some of the images that we were able to collect are depicted in the following figures.
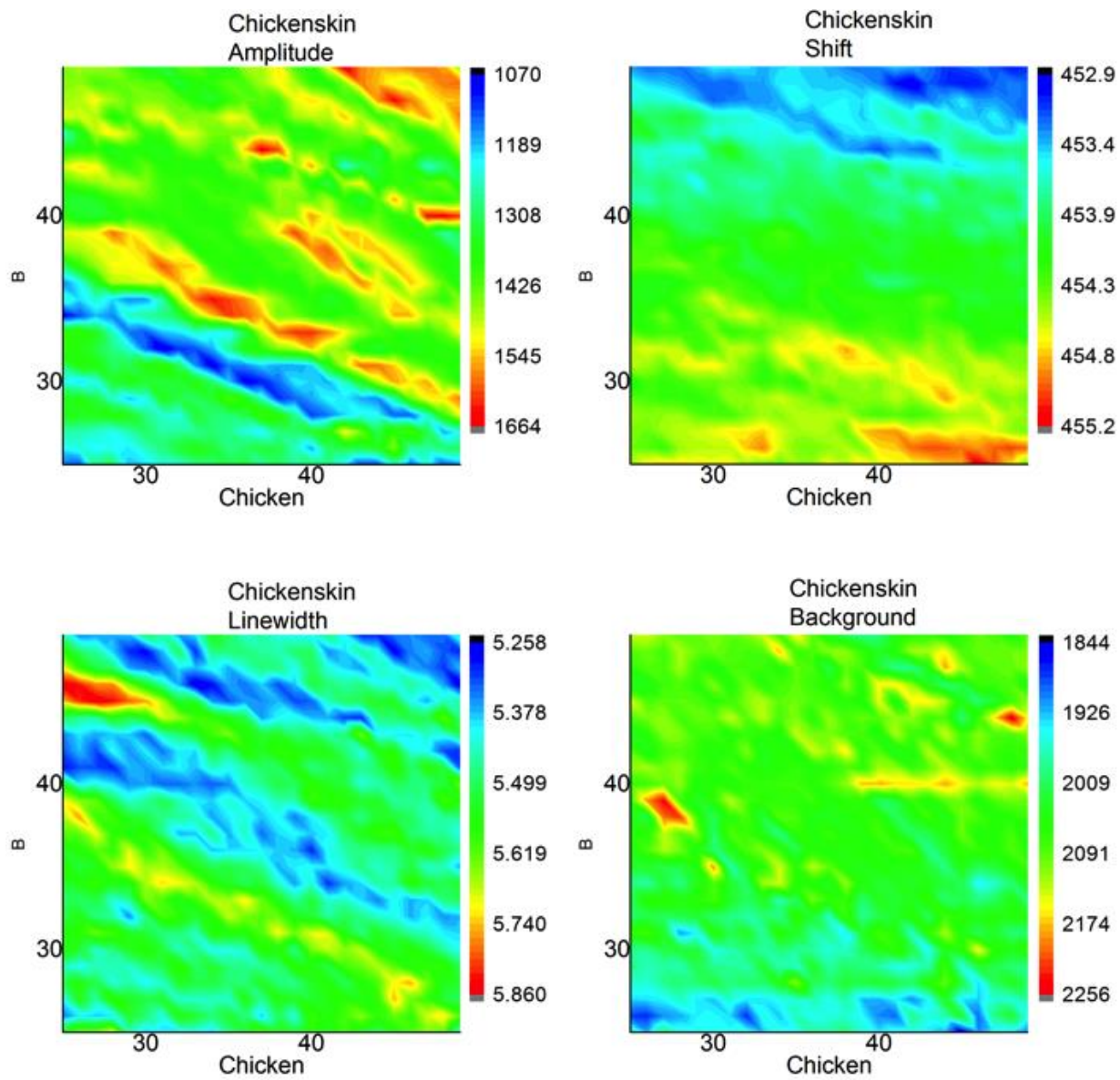
Figure 8: Brillouin images created depicting various spectral information, including Brillouin amplitude, shift, linewidth, and background signal across a 50x50 micron chicken skin section, resolution 2 microns.
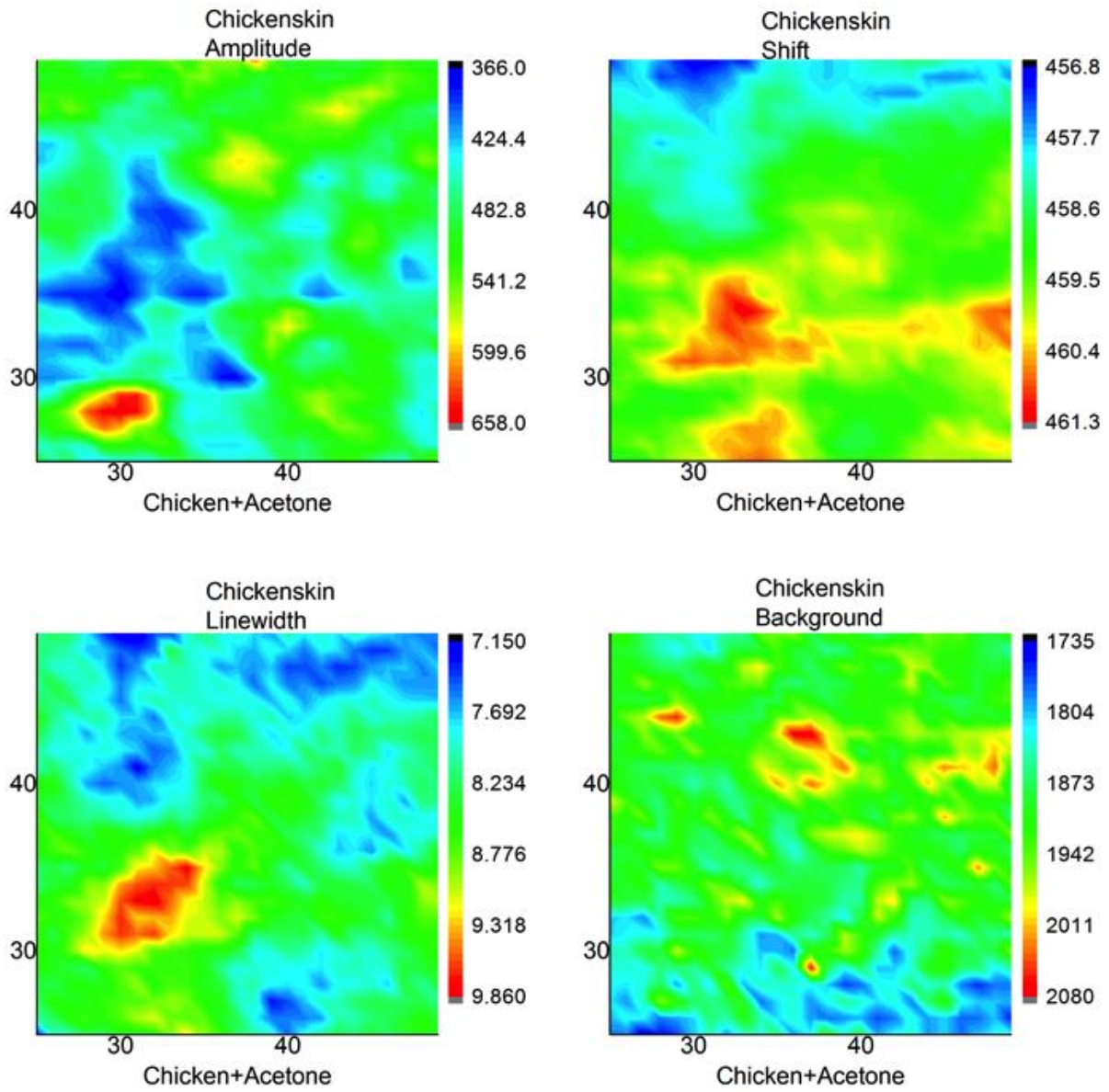
Figure 9: Chicken skin sample from Figure 8, this time treated with acetone. Note that the Brillouin shift increases with treatment (tissue becomes stiffer).
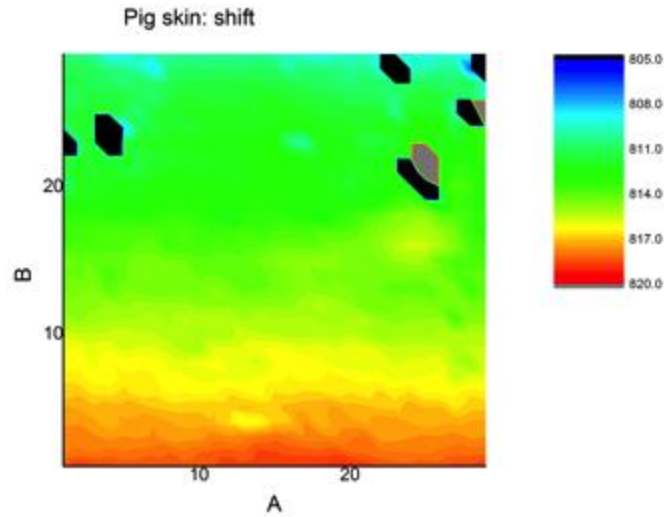
Figure 10: Pig skin, mapped on a 30x30 micron section. Laser drift (increasing down the sample) is clearly apparent and hinders the creation of a good image.

Thus, we have created Brillouin images using only the setups previously employed, plus a micro-scale translation stage. Improvements in laser stability need to be made in order to keep the images at a high quality, as depicted in Figure 10 above.

CHAPTER IV

DISCUSSION

In summation, we have developed and discussed Brillouin spectroscopy in a number of ways. We found a new application; applying Brillouin spectroscopy towards the diagnosis of bacterial meningitis by detecting increased CSF protein levels. We also determined a method of improving Brillouin spectrum acquisition by the use of molecular absorption cells acting as a notch filter for elastically scattered light. Finally, we created Brillouin images, or "modulus maps," of tissues using a laser scanning method. While our Brillouin imaging technique is still in its early stages and could use some improvements, this still represents a significant step forward in terms of microscale mechanical interactions and the monitoring of the biomechanics of cellular interactions. Brillouin spectroscopy has an enormous ceiling in terms of the information that it is capable of providing, and it is only development of the technology, via undertakings such as those presented in this thesis, that are holding progress from rapid advancement forward.

REFERENCES

Bailey, S. T., M. D. Twa, J. C. Gump, M. Venkiteshwar, M. A. Bullimore and R. Sooryakumar (2010). "Light-Scattering Study of the Normal Human Eye Lens: Elastic Properties and Age Dependence." Biomedical Engineering, IEEE Transactions on **57**(12): 2910-2917.

Bilaniuk, N. and G. S. K. Wong (1993). "Speed of sound in pure water as a function of temperature." The Journal of the Acoustical Society of America **93**(3): 1609-1612.

Brouwer, M. C., G. E. Thwaites, A. R. Tunkel and D. van de Beek "Dilemmas in the diagnosis of acute community-acquired bacterial meningitis." The Lancet **380**(9854): 1684-1692.

Carman, J. C. (2012). "Classroom measurements of sound speed in fresh/saline water." Journal of the Acoustical Society of America **131**(3): 2455-2458.

El Bashir, H., M. Laundy and R. Booy (2003). "Diagnosis and treatment of bacterial meningitis." Archives of Disease in Childhood **88**(7): 615-620.

Engler, A. J., S. Sen, H. L. Sweeney and D. E. Discher (2006). "Matrix Elasticity Directs Stem Cell Lineage Specification." Cell **126**(4): 677-689.

Enwere, G. E. and S. K. Obaro (2001). "Diagnosis of bacterial meningitis." The Lancet **358**(9292): 1549.

Haidong, G., D. Huijuan, Z. Guangyu, H. Jun and P. Hongliang (2013). "Effects of Polymer Coatings on Temperature Sensitivity of Brillouin Frequency Shift Within Double-Coated Fibers." Sensors Journal, IEEE **13**(2): 864-869.

Hirschberg, J. G., J. D. Byrne, A. W. Wouters and G. C. Boynton (1984). "Speed of sound and temperature in the ocean by Brillouin scattering." Applied Optics **23**(15): 2624-2628.

Karlsson, B. and C. Alling (1980). "A comparative study of three approaches to the routine quantitative determination of spinal fluid total proteins." Clinica Chimica Acta **105**(1): 65-73.

Leyendekkers, J. V. (1977). "Prediction of the refractive index of seawater as a function of temperature, pressure, salinity and wavelength." Marine Chemistry **5**(1): 29-42.

Metsämuuronen, S., M. Mänttäri and M. Nyström (2011). "Comparison of analysis methods for protein concentration and its use in UF fractionation of whey." Desalination **283**(0): 156-164.

Mongelluzzo, J., Z. Mohamad, T. R. Ten Have and S. S. Shah (2008). "COrticosteroids and mortality in children with bacterial meningitis." JAMA **299**(17): 2048-2055.

Monkos, K. (2005). "A comparison of solution conformation and hydrodynamic properties of equine, porcine and rabbit serum albumin using viscometric measurements." Biochimica et Biophysica Acta (BBA) - Proteins and Proteomics **1748**(1): 100-109.

Pennock, C. A., L. P. Passant and F. G. Bolton (1968). "Estimation of cerebrospinal fluid protein." Journal of Clinical Pathology **21**(4): 518-520.

Pfister, H., W. Feiden and K. Einhäupl (1993). "Spectrum of complications during bacterial meningitis in adults: Results of a prospective clinical study." Archives of Neurology **50**(6): 575-581.

Richerzhagen, B. (1996). "Interferometer for measuring the absolute refractive index of liquid water as a function of temperature at 1.064 μm." Applied Optics **35**(10): 1650-1653.

Sathyavathi, R., N. C. Dingari, I. Barman, P. S. R. Prasad, S. Prabhakar, D. Narayana Rao, R. R. Dasari and J. Undamatla (2013). "Raman spectroscopy provides a powerful, rapid diagnostic tool for the detection of tuberculous meningitis in ex vivo cerebrospinal fluid samples." Journal of Biophotonics **6**(8): 567-572.

Scarcelli, G., S. Scarcelli and Yun (2011). "Multistage VIPA etalons for high-extinction parallel Brillouin spectroscopy." Optics express **19**(11): 10913.

Stuertz, K., I. Merx, H. Eiffert, E. Schmutzhard, M. Mäder and R. Nau (1998). "Enzyme Immunoassay Detecting Teichoic and Lipoteichoic Acids versus Cerebrospinal Fluid Culture and Latex Agglutination for Diagnosis of Streptococcus pneumoniae Meningitis." Journal of Clinical Microbiology **36**(8): 2346-2348.

Swartz, M. N. M. D. (2004). "Bacterial Meningitis - A View of the Past 90 Years." The New England Journal of Medicine **351**(18): 1826-1828.

Tunkel, A. and W. M. Scheld (2002). "Treatment of bacterial meningitis." Current Infectious Disease Reports **4**(1): 7-16.

Wang, S. H., L. P. Lee and J. S. Lee (2001). "A linear relation between the compressibility and density of blood." The Journal of the Acoustical Society of America **109**(1): 390-396.